Studies on the Texture of Nematic Solutions of Rodlike Polymers. 2. Development and Relaxation of Loop Disclinations

Zhanjie Tan, Beibei Diao,[†] and Guy C. Berry*

Department of Chemistry, Carnegie Mellon University, Pittsburgh, Pennsylvania 15213

Received May 24, 1999; Revised Manuscript Received August 17, 1999

ABSTRACT: Features of the development and relaxation of loop defects in the texture of nematic solutions of two rodlike polymers are discussed. Examples given for solutions of poly(1,4-phenylene terephthalamide) and poly(1,4-phenylene-2,6-benzobisthiazole) show the overall similarity of the behavior for these two materials. The development of the mottled texture observed shortly after the solution is extruded into a rectangular capillary, to form a tangle of defect lines which then evolves to form individual loops, is discussed. The differing relaxation dynamics of individual loops observed in the final stages of coarsening near the cell center and close to a surface are presented, along with novel effects observed in the interaction of such loops with an external magnetic field.

Introduction

Loop defects that enclose an area that decreases with increasing time are often seen during the latter stages of the coarsening of nematic fluids to a defect-free state.[1−16] These defects are usually interpreted as type $s = {}^1/_2$ twist loops, and their relaxation dynamics have been the subject of theoretical treatments.[17−25] Studies have also included certain effects of external magnetic fields on nematogens with diamagnetic anisotropy.[26−30] It was reported that defects with the appearance of type $s = {}^1/_2$ twist loops were found near, and nearly parallel to but not attached to, the confining surfaces, and were not to be found in the interior of the fluid in the final stages of the relaxation of loops in nematic solutions of poly(1,4-phenylene-2,6-benzobisthiazole), PBZT.[13] In the latter study, the area $A(t)$ enclosed by these loops relaxed as the square of the time Δt remaining for the disappearance of the loop, i.e., $[A(t)]^{1/2} \propto \Delta t$. By contrast, a computer simulation of the relaxation of a twist loop gave $A(t) \propto \Delta t$ behavior,[21] with similar behavior expected theoretically with some models,[12,17,20,21,25] and reported with small molecule nematogens[9−12] and thermotropic nematics.[15,16] Of course, the time for the loop disappearance is much longer with polymeric nematics than the few seconds typical for small molecule nematogens.

The differing relaxation dynamics of individual loops observed with nematic solutions of rodlike polymers in the final stages of coarsening near the cell center and close to a surface will be presented in this study, along with novel effects observed in the interaction of such loops with an external magnetic field. Examples will include loop defects in nematic solutions of poly(1,4-phenylene terephthalamide), PPTA, including behavior at an earlier time in the late stages of coarsening than reported in the study on PBZT. In addition, the relaxation of the tangle of defect lines observed at a certain stage in the coarsening process, and the effects of an external magnetic field on the structure of well-defined loops will be discussed, using examples obtained with nematic solutions of PBZT. Prior work on the effects of

an external magnetic field on defect-free preparation of nematic solutions of PBZT have included investigations of the uniform[31] and nonuniform[32] distortions of the director.

Experimental Section

Nematic solutions were prepared by dissolving the vacuum-dried polymer in the appropriate solvent under dry conditions, it being essential to rigorously exclude moisture to suppress aggregation of the polymer.[13,31−34] The solutions of PBZT in methanesulfonic acid (MSA) used in this study are described in part 1 of this series.[31] The PPTA solutions were prepared with samples recovered from Kevlar fiber (Kevlar 29) kindly provided by Dr. S. R. Allen, Advanced Fiber Systems, Du Pont Co., Inc., Richmond, VA. The fiber was refluxed with acetone and water in a Soxhlet extractor successively for 48 h each and dried under vacuum. The dry polymer was dissolved in 96% sulfuric acid (Fisher) to give ≈1 g/L, followed by rapid precipitation in a large excess of deionized water (≈0 °C). The precipitate was exhaustively rinsed in deionized water, freeze-dried to remove almost all of the water, and then dried under high vacuum (0.001 mmHg) for 2 weeks immediately prior to use. The intrinsic viscosity $[\eta]$ of the Kevlar 29 used is 740 cm³/g as determined in the concentration range 0.025−0.1 g/dL in 100% sulfuric acid. The 100% sulfuric acid was prepared by titrating fuming sulfuric acid (from Aldrich) with 96% sulfuric acid (from Fisher) to the end point for which the addition of the 96% acid did not produce fumes, giving a sulfuric acid content ≈99.8−100%. Lyotropic solutions of PBZT in MSA or PPTA in 100% sulfuric acid were prepared by addition by weight of polymer and solvent to a 35 mL centrifuge tube containing a Teflon-coated magnetic stirring bar, under a dry nitrogen (ultrahigh purity) atmosphere. The sealed tubes were slowly rotated between the poles of a horseshoe magnet for a period of 2−3 weeks to form a homogeneous solution at room temperature. Since Kevlar 29 was found to degrade in solutions of 100% sulfuric acid at temperatures above 100 °C, all studies were confined to temperatures below 60 °C. It was found that attempts to dissolve PPTA in 96% sulfuric acid or MSA did not lead to stable homogeneous nematic solutions at the concentrations of interest here. For example, solutions of PPTA in 96% sulfuric acid were isotropic at polymer concentrations up to $w = 0.12$, probably due to intermolecular association, similar to effects reported with PBZT caused by intrusion of moisture to an initially nematic solution.[31,35] For higher concentrations up to $w = 0.15$, the solution contained gray particles, perhaps representing a crystal solvate.[36−41]

---

* Address for correspondence.
† Current address: Du Pont Co., Inc., Buffalo, NY.

Table 1. Parameters for Nematic Solutions

| polymer	weight fraction, w	$[\eta]$ (cm³/g)	contour length^a L_w (nm)	η_{ss} (Pa·s) (slow flow)^b	$T_{NI}{}^c$ (°C)	$w/w_{NI}{}^c$	cell thickness used (μm)
PPTA	0.083	740	235		≈15		400
PPTA	0.0976	740	235	955	≈45		400
PPTA	0.105	740	235		>60		100, 400
PPTA	0.120	740	235	620	>60		100, 400
PBZT	0.0634	1400	135	2480	147		300
PBZT	0.0581	1800	155	150	117.₅	1.87	300
PBZT	0.049	1800	155	2000		1.47	200

^{a} Estimated from $[\eta]$ using the following expressions: $L_w/\mu m = 2.41([\eta]/mL\cdot g^{-1})^{5/9}$ for PBZT in methanesulfonic acid,[42] and $L_w/\mu m = 3.98([\eta]/mL\cdot g^{-1})^{1/1.62}$ for PPTA in sulfuric acid.[43-45] ^{b} Slow flow refers to a regime of shear rate for which the steady-state viscosity η_{ss} is independent of the shear rate. ^{c} T_{NI} is the temperature for the nematic−isotropic transition at the listed w, and w_{NI} is the weight fraction for which the transition occurs at the temperature used in the loop study.

After dissolution was complete, the nematic solution was extruded into a rectangular channel, and sealed to prevent contamination by moisture. The cells used in this study have been described elsewhere.[32,33] Briefly, Luer tips were attached to both ends of a section of rectangular tubing (Vitro Dynamics, Rockway, NJ), 1−2 cm long, 0.5 cm wide, and from 100 to 500 μm thickness (constant for any given channel). The nematic solution could then be extruded into the cell through a Teflon tube connected to one of the Luer tips, with the other tip connected to a drying tube. The Teflon tube extended into the sealed sample tube, which was pressurized with dry nitrogen to extrude the sample into the cell. After the cell was filled, the Luer tips were capped with a Luer cap, and sealed with an epoxide. The sealed cells were kept in a desiccator when not in use as a precaution, but the cells would usually protect the sample from intrusion by moisture over a period of years. Concentrations are expressed as weight fraction, w, or as weight percent (100w) unless otherwise noted. Parameters for the solutions examined are given in Table 1, based on correlations in the literature.[42-45]

A polarizing microscope (Leitz) equipped with a CCD camera (Panasonic BL202) was used for microscopy, with most observations being made at room temperature (≈25 °C). The microscope stage was equipped with a temperature controller (Mettler FP 5 with hot stage Metler FP 52). Light sources used included a polychromatic tungsten bulb, the blue (436 nm) or green (541 nm) emission from a mercury lamp, and a plane-polarized He−Ne laser (Melles Griot; 15 mW, 633 nm). The microscope could be used to observe the polarized fluorescence emission from a beam incident on the top surface of the sample. Most of the orthoscopic observations utilized the tungsten lamp, with occasional use of the mercury source for (nearly) monochromatic imaging. Both orthoscopic and conoscopic examination utilized the laser, with a rotating, slightly turbid film placed in the incident light beam below the condensing lens to essentially destroy the coherence of the laser beam. The optical images from the CCD camera were recorded by a videotape recorder (RCA, VR 452), and the images were processed using a frame grabber (Video Player) on a Power Macintosh (7600/132). Some images were taken with a 35 mm camera to achieve better resolution and contrast; these images were scanned to produce a copy for processing.

Results

Textural Observations. The textures of the PBZT and PPTA solutions were qualitatively similar in most respects. A principal difference in their qualitative appearance being that the PBZT solutions exhibited more dichroism than the PPTA solutions as the samples approached a defect-free texture. With either polymer, the texture immediately after extrusion into a cell was essentially independent of the cell thickness. The fluorescence emission intensities $I_\parallel$ and $I_\perp$ along and perpendicular to the flow direction, respectively, from a slab of the nematic near the cell surface provide some insight
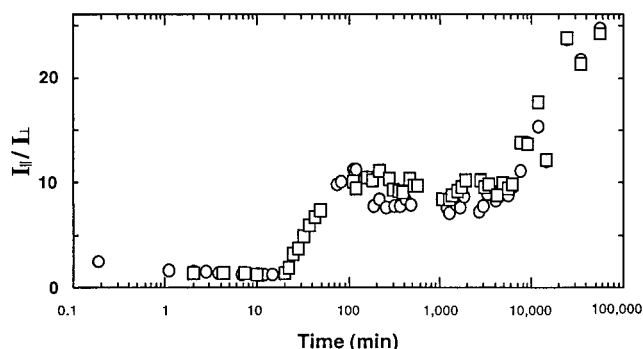
Figure 1. The ratio of the fluorescence emission intensities $I_\parallel$ and $I_\perp$ between parallel and crossed polars, respectively, for a coarsening nematic PBZT solution following extrusion into a cell with a rectangular cross-section (400 μm × 8 mm). The fluorescence arises from incident radiation absorbed within ≈1 μm of the surface.

on the initial alignment and its development with coarsening. Examples of the ratio $I_\parallel/I_\perp$ of the fluorescence emission are given in Figure 1 for samples of PBZT on annealing following extrusion into a parallel cell 400 μm thick.[13] Since the 436 nm wavelength incident light used is strongly absorbed (i.e., 99% absorption within 1 μm), the fluorescence emission is a measure of the orientation close to the surface.[13,46] The anisotropy near the surface detected by the fluorescence emission is small, but not zero, immediately after the flow is stopped and indicates a preferential alignment along the flow direction near the cell surface in the filling process. The fluorescence emission increases to an intermediate plateau after about 1 h, but the increase to the final high level of anisotropy in the fluorescence emission characteristic of the monodomain and the uniformity of director alignment along the extrusion direction necessary to form conoscopic interference figures were not observed until more than 70 days after the cell was filled.

The texture corresponding to the fluorescence development included the an initial rather mottled appearance, followed by the development of diffuse bands, which gradually evolved to a net of line defects. The initial texture, shown in Figure 2a for a nematic solution of PBZT, displayed a sinuous birefringence pattern, with superposed bands perpendicular to the extrusion direction, which will be referred to hereafter as the cell axis. Similar band structures were observed for PPTA, both in the cell used here, and after loading samples into a torsional rheometer in work to be described in part 3 of this series. After some time, an intermediate texture shown in Figure 2b developed, with diffuse bands that would eventually develop the tangle of line defects discussed below.
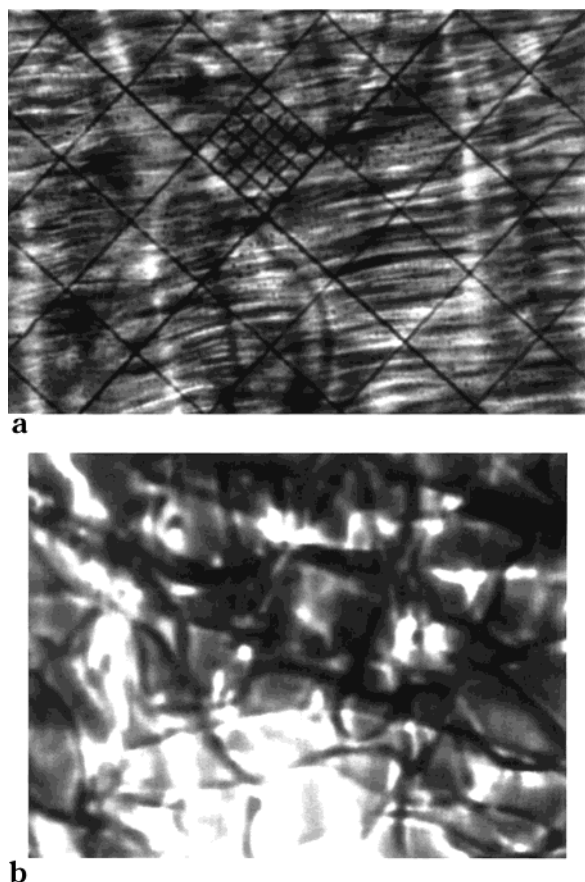
Figure 2. Micrographs of a nematic solution of PBZT at different times after extrusion into the cell, and before line defects are well developed. Both images are between crossed polars. The polarization of the incident beam is oriented at 45 degrees to the horizontal, which is the extrusion direction in the cell. Key: (a) solution shortly after extrusion into the cell, showing a sinuous pattern in the birefringence along the flow direction, with superposed images precursors to loop defects orthogonal to that direction; (b) precursors to the line defects observed about a day after extrusion. These will subsequently develop to form a net of defect lines. 80 μm/div.

The texture 12 h after loading depended on the cell thickness and the polymer, with the texture coarsening most rapidly with solutions of PPTA in a thin cell. For example, after being annealed for about 12 h, the texture of either PPTA solutions in the 400 μm cell or PBZT solutions in 200 or 300 μm cells was complex, showing the precursor to a tangle of disclination lines that developed at a later time, superposed on a sinuous striated texture in the bulk of the cell. By contrast, after the same interval, the texture of the solution of PPTA in the 100 μm cell ($w = 0.0976$) coarsened to suppress all line defects and exhibited relatively diffuse interference bands parallel to the extrusion direction, when viewed under crossed polars with laser light with the fringes. The fringes became sharper and more numerous with increasing time, and well-defined conoscopic images could be observed after about 24 h. The fringes observed orthoscopically are attributed to nonuniformity in thickness across the cell, with an increase in the number of fringes over time due to an increase in the alignment of the nematic field, resulting in a corresponding increase in the optical retardation through the thickness of the cell. The conoscopic interference patterns were symmetric, similar to those reported in prior work on PBZT.[32,46,47] Following methods described elsewhere,[33] calculations gave $(n_E - n_O)/c \approx 0.16$ mL/g,

with n_E and n_O being the extraordinary and ordinary refractive indices, respectively. This result was obtained for a sample after several weeks of annealing, at which time the sample was defect-free, with interference figures that appeared not to be changing with time. Similar behavior was observed with solutions of PBZT[13] and with PPTA in thicker cells, but on a longer time scale.

Although, as noted above, the texture in the bulk in the thicker cells (>200 μm) was complex after 12 h, a more ordered texture was observed near the edges of the cell with PPTA in a 400 μm cell ($w = 0.0976$). Thus, white light was extinguished between crossed polars near the edges of the cell, with the polarizer along the cell axis. With a laser light source, a series of fringes was observed near the edges of 400 μm cells containing the PPTA solution, with concentric elliptically shaped fringes merging into the cell center, with the fringes more closely spaced toward the cell center; these are associated with a weak tendency to form bands orthogonal to the cell axis.

Several days after loading, the texture in the thicker cells on nematic PPTA solutions coarsened to reveal a tangle of line defects immersed in a strongly birefringent matrix; the appearance is similar to that noted for nematic solutions of PBZT[13] and small molecule nematogens[10,48] Even though the matrix is birefringent at this stage and appears to be aligned in the flow direction when viewed with white light between crossed polars, it does not support conoscopic interference figures, and complex fringe patterns can be observed in the matrix regions using orthoscopic microscopy with a laser or a mercury arc line as the light source. Thus, the matrix is misaligned by weak but pervasive and geometrically complex gradients in the director field around the line defects. As shown in Figure 3, for a solution of PBZT ($L_w = 135$ μm; $w = 0.0581$), the tangle exhibits a preponderance of relatively sharply defined line defects, similar in appearance to type $s = 1/2$ twist loop defects, and a smaller number of more diffuse, relatively straight defects, similar in appearance to type $s = 1$ twist defects. These same features are evident when viewed with polarized light either with or without an analyzer. As shown in Figure 3, the straight line defects were the first to disappear as both the tangle simplified and the area enclosed by a given loop decreased with increasing time. With increasing coarsening, the elliptical fringes noted above remained near the cell edges, with a fine fringe pattern associated with the line defects developing throughout as the defect pattern coarsened.
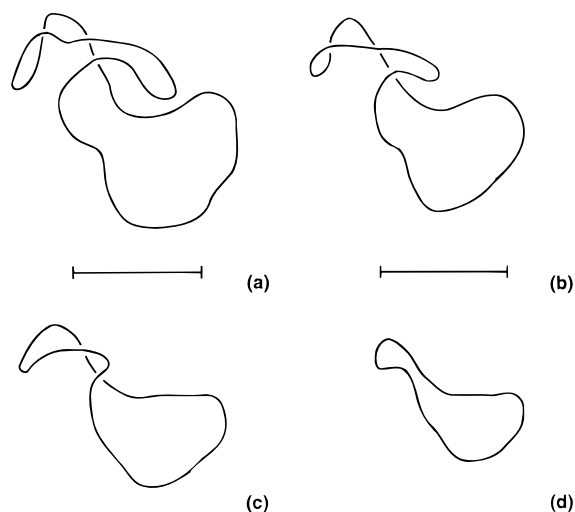
After about 2 weeks, the texture in the 400 μm cells of PPTA nematic solutions coarsened so that isolated, noncrossing closed line defect loops were the dominant defect texture, superposed on a smooth, strongly birefringent background, with extinction between crossed polars with a polarizer oriented along the cell axis. Dichroism measurements show this to be the direction for the strongest absorption in the visible, confirming that the molecular axis is preferentially along the cell axis. The optical features of these line defects have been described in detail elsewhere.[13] At this stage, no vestige remained of the bands observed immediately after filling the cell. In no case was a knotted line defect loop observed, although, not infrequently, a loop would be nonplanar, writhing about itself in three dimensions.[13] The patterns in Figure 4 show an schematic drawing of an example observed with a PPTA solution ($w = $
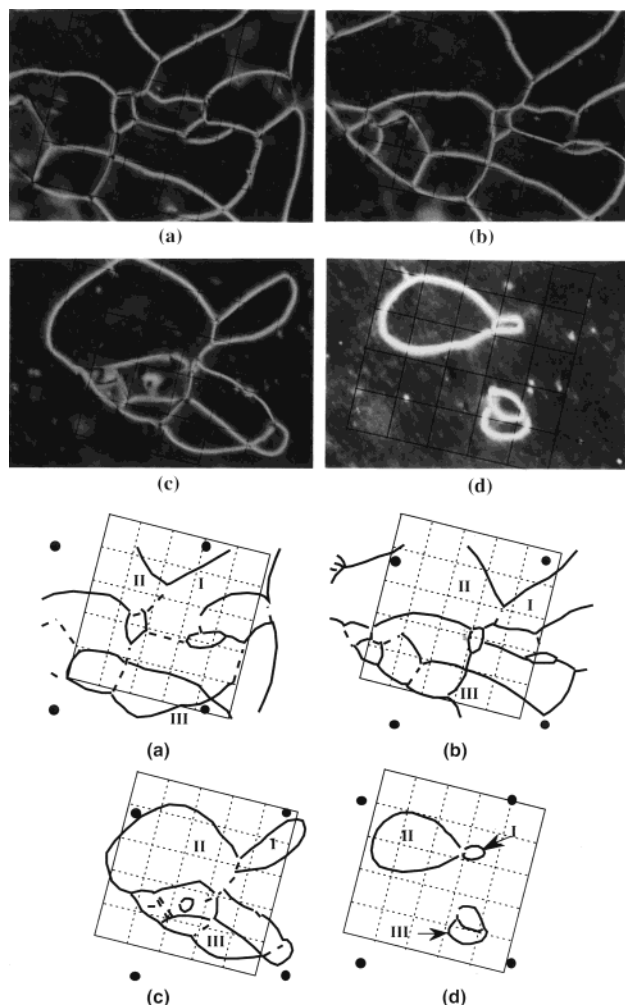
Figure 3. Relaxation of a net of defect lines toward isolated loops in a nematic solution of PBZT. The images in parts a-— were observed at 71, 89, 161, and 245 h, respectively, from the time the cell was filled. Key: (i) micrographs obtained between crossed polars; (ii) schematic drawings of the micrographs. The filled circles mark an area approximately the same in all figures. The roman numerals mark regions within loops as they evolved with time. 53 μm/div.


Figure 4. Schematic drawings traced from a nonplanar loop defect in a nematic PPTA ($w = 0.12$) as it relaxes to a smaller, planar loop. Note that portions of the loop pass closely, but do not touch, during this process. The images b—d were taken at 21, 48, and 83 h, respectively, following the first image. The arrow marks 130 μm.

Figure 5. Micrograph of nonplanar loops viewed between crossed polars, oriented at 45 degrees to the preferred orientation (the extrusion direction), which is along the diagonal of the image. Conditions: PPTA; $L_w = 235$ μm; $w = 0.105$; 400 m thick cell.

0.120) of a line defect that writhed about itself several times, without actually forming a knot; photographic images and schematic drawings of a similar, but more complex, relaxation of a writhed loop may be found in Figure 8 of a prior publication on PBZT.[13] For both PPTA and PBZT solutions, such nonplanar loops tended to unwrithe and flatten into a planar two-dimensional shape, without ever crossing, see Figures 4 and 5. The drawings in Figure 4 were traced from successive images as the area enclosed by the loop decreased and the loop tended to become planar; the out-of-plane character was determined using the depth-of-field of the microscope. The image in Figure 5, exhibits a few nonplanar, but isolated, loops viewed in orthoscopic microscopy between crossed polars, oriented at 45° from the preferred direction for orientation (the extrusion direction); various portions of these loops could be brought into focus at different depths in the sample. The loops exhibit alternating bright and dark banding, similar to the pattern observed with loops in nematic solutions of PBZT,[13] with superposed fringe patterns, representing variations in the birefringence, superposed on the loop structure.

At an advanced stage in the coarsening, most of the loops were isolated, nearly planar, and in the plane of the cell. At this stage, the defect loops were excluded from a slab of thickness $\approx 50-100$ μm extending from either surface but were otherwise approximately evenly distributed in the cell. Observation between crossed polars with a laser light source revealed coarsened fringe patterns in the vicinity of the lines, with widely variable fringe spacing from place-to-place in the cell. These fringe patterns reveal a complex character for the order tensor at this stage, despite the well developed birefringence in orthoscopic microscopy. After about a month, almost of the line defect loops remaining in the 400 μm cell with nematic solutions of PPTA were only found in layers about $50-100$ μm from the confining surfaces, with the plane of the loop essentially parallel to a surface, and as with the solutions of PBZT.[13] In subsequent coarsening, the loops decreased in area, but did not migrate otherwise. Very coarse fringe patterns could be seen between crossed polars under laser light illumination in a few places in the cell. In the final stages of texture coarsening, distorted conoscopic interference patterns could be observed in regions of the cell
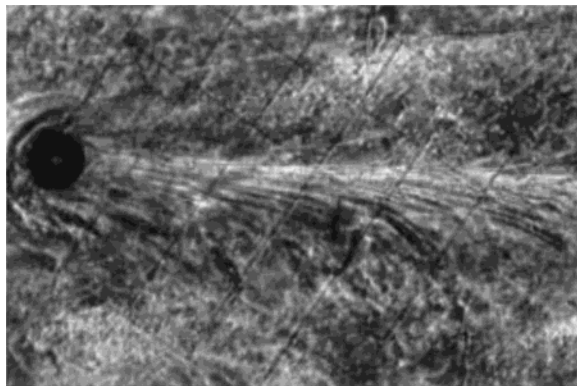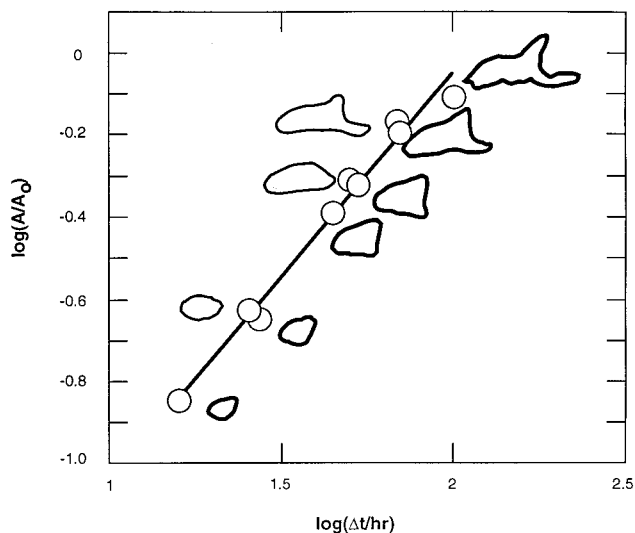
Figure 6. Defect lines during the translation of a bubble in a nematic solution of PPTA; the bubble motion is toward the left in the image, which is between crossed polars. The polarization of the incident beam is oriented at 45° to the horizontal, which is the extrusion direction in the cell. 80 μm/div.

Figure 7. Schematic drawings of the shape changes during the collapse of the area A enclosed by an initially irregularly shaped loop in a nematic solution of PPTA. Δt is the time remaining for disappearance of the loop, and A_0 is the area of the loop at the start of the observation, with a long dimension of about 400 μm. Open loops were those observed, and hatched loops were calculated for relaxation by curvature.

characterized by a sparse density of line defect loops.

In a few cases, bubbles were entrapped in the cell. A family of line defects formed in the wake of such bubbles if they were allowed to rise in the cell, similar to the behavior reported for small molecule nematogens;[49] see Figure 6. In these cases, the bubble motion, caused by a slight orientation of the cell plane out of the horizontal plane (<5°) was slow, $\approx$0.5 μm/s. Not all bubbles moved at the same rate, perhaps reflecting their size or the complexity of the texture around them. In some cases, a relatively stable loop was observed in the wake of a translating bubble, similar in structure to stable loops observed if a partially coarsened sample is placed in a magnetic field,[13,32] These loops are elliptical in shape, but with sharp apexes, and have the appearance of two type $s = 1$ lines joined at the apexes of the elliptical loop, as may be seen in figures in the references cited.

Coarsening Dynamics of Defect Loops. The size and shape of the line defect loops in the 400 μm cells were followed after the coarsening to form isolated loops. Only isolated, nearly planar loops with the appearance of type $s = 1/2$ twist loops with the loop plane (essentially) in the plane of the cell were used in this analysis. Observations were begun at a stage in which these isolated loops could be found essentially evenly distributed throughout the cell, except within a distance less than 50−100 μm from the cell walls; no line defects were observed within that space. At this stage, the fringe pattern observed between crossed polars with the laser light source reveals a very complex order tensor in the bulk of the sample, with the alignment varying over micrometer dimensions. The marked birefringence observed for the background of the loop defects is attributed to a more well-aligned structure near the surfaces, such that adiabatic propagation of light in orthogonal microscopy reveals only information on the alignment near the cell surfaces.[13] Thus, for example, conoscopic images could not be obtained from the cell at the time that loops were distributed throughout the cell, despite the strong birefringence. As with solutions of PBZT,[13] with increased annealing time, the loops in the bulk of the nematic shrank and disappeared, so that the final loops seen were found only near the cell surfaces (within 50−100 μm), and at this stage, somewhat distorted conoscopic images could be observed from areas far from loop defects, indicating that the nematic was approaching a well-aligned monodomain structure except near the defect loops.

Although many of the loops were nearly elliptical during the time observed, several were observed from a time when they had a very irregular shape. An example of the change in shape with coarsening time and relaxation of the loop area for an initially irregularly shaped loop in a nematic solution of PPTA is shown in Figure 7; this loop was near the cell midplane. In all cases, the shape tended to become elliptical and then circular with increasing time, until the loop became too diffuse to be clearly resolved, acquiring a radius of $\approx$ 5 μm or less. The distance of the loop plane from the surfaces remained constant during the relaxation of the loop area. The area $A(t)$ of the loop at time t elapsed after the sample was extruded into the cell was determined by either or both of two methods, both based on prints of the expanded images of the loop and a superposed grid in the microscope optics recorded with the CD camera: (1) the expanded images of loop and grid were cut from the print and weighed, and the area of the loop was calculated using the known dimension of the grid; (2) for loops nearly elliptical in shape, the maximum and minimum dimensions of the figure were determined by measurements on the print and used to compute the area assuming the figure to be an ellipse. These methods were found to be in good agreement when both were applied to a nearly elliptically shaped figures. In a few cases, a freeware application (WinDIG, Version 2.5) was also used to determine the area of an irregularly shaped figure, with good agreement with the area determined by the weight method.

In analyzing the loop relaxation dynamics, data on $A(t)$ and $[A(t)]^{1/2}$ vs t' were examined to determine whether either function was approximately linear, and if so, the time t_0' for relaxation of $A(t)$ to zero was estimated, where $t' = t - t_{st}$ with t_{st} the (arbitrary) time measurements were begun; both t and t_{st} are measured from the time the sample was extruded into the cell. Plots of $\log[A(t_0' - t')]$ vs $\log[t_0' - t']$ were then examined for power-law behavior, using the estimation of t_0' from the relevant linear analysis in the first step of an iteration to obtain the best fit by linear regression with

Table 2. Loop Relaxation Data

	$\Delta d/\mu m$ (Proximity to a surface)	t_{st}/min (Time to start observation)	t_o/min (Time loop disappeared)	$A(t_{st})/(\mu m^2)$ (Loop area at time t_{st})	Loop shape at time t_{st}	$\dfrac{\partial \ln[A(t)]}{\partial \ln(\Delta t)}$ $\Delta t = t_o - t$
1	120 (bottom)	22,050	13,750	1,124	Elliptical	1.06
1	175 (bottom)	25,753	26,247	4,823		1.22
1	175 (bottom)	27,205	25,793	3,309		1.01
1	165 (top)	27,205	68,795	4,313		0.96
1	165 (top)	27,205	47,795	2,853		1.00
1	100 (bottom)	27,206	112,794	13,908		2.01
1	100 (top)	110,000	250,000	8,250	Elliptical(1.23)	2.01
1	100 (top)	110,000	235,000	8,000	Elliptical(1.29)	2.01
1	115 (bottom)	117,000	200,000	3,300	Irregular	2.07
1	115 (bottom)	110,000	240,000	12,150	Elliptical(1.88)	2.01
1	120 (bottom)	110,000	180,000	2,300	Irregular	2.10
1	120 (bottom)	110,000	200,000	7,850	Irregular	2.09
1	120 (bottom)	110,000	290,000	12,000	Irregular	2.02
1	140 (bottom)	110,000	250,000	8,900	Elliptical(1.75)	2.01
1	140 (bottom)	110,000	275,000	7,400	Irregular	2.00
2	≈ 200	$\approx 20,000$	5,700	30,000		1
2	≈ 200	$\approx 20,000$	40,000	$\approx 800,000$		1
2	$\approx 50\text{-}100$	$\approx 85,000$	42,000	6,400	Elliptical(1.61)	2.00*
2	$\approx 50\text{-}100$	$\approx 85,000$	25,000	5,100	Elliptical(2.00)	1.98*
2	$\approx 50\text{-}100$	$\approx 85,000$	11,000	2,200	Elliptical(1.45)	2.24
2	$\approx 50\text{-}100$	$\approx 85,000$	52,000	10,900	Elliptical(1.89)	2.02
2	$\approx 50\text{-}100$	$\approx 85,000$	40,000	10,500	Elliptical(2.21)	1.75*
2	$\approx 50\text{-}100$	$\approx 85,000$	23,000	5,200	Elliptical(1.03)	2.15
2	$\approx 50\text{-}100$	$\approx 85,000$	48,000	12,300	Elliptical(1.20)	2.02
3	≈ 200	$\approx 25,000$			Elliptical	...**
3	≈ 200	$\approx 25,000$	1,685	7,359	Elliptical	1
3	≈ 200	$\approx 25,000$	5,331	1,961	Elliptical	1.5
3	≈ 200	$\approx 25,000$	1,389	735	Elliptical	2

1: 9.76% K29 in sulfuric acid   Cell thickness was 400 microns.
2: 10.5% K29 in sulfuric acid   All loops contracted toward elliptic form; tending
3: 12.0% K29 in sulfuric acid   toward circular.
*   Power-law behavior not followed for very small area at long times
** No power-law behavior

t'_0 as a variable, with the exponent

$$\nu = \partial \ln[A(t'_0 - t')]/\partial \ln[t'_0 - t'] =$$
$$\partial \ln[A(t_0 - t)]/\partial \ln[t_0 - t] \quad (1)$$

being the parameter of interest. The initial and final estimates of t'_0 did not differ much, and in most cases, the best fits were obtained with values of ν close to either 1 or 2; see Table 2. As noted in Table 2, in several cases, the plots of $A(t')$ or $[A(t')]^{1/2}$ vs t' showed that the data were best described by two lines, for shorter and longer t'; see Figure 8, in which the data at long times may be seen to deviate from the straight line fit to the data at shorter times. Such data could not be fitted by a single power-law expression with any value of t'_0. Consequently, as noted in Table 2, the data for the larger $A(t')$, and the corresponding t'_0 estimate are reported here. The data at longer t' could always be fit by a power-law with the same ν found at shorter times, but with a much smaller prefactor, reflecting the decreased relaxation rate. This behavior may relate to a reduced rate of reorientation of the director field in the plane enclosed by the loop in the final stages of the coarsening.

Distortion in a Magnetic Field. The aromatic rings in the PBZT and PPTA structures provide a source of anisotropy for the magnetic susceptibility tensor, such that the chains will tend to align with their molecular axes parallel to the direction of an applied external magnetic field.[31,32,47] This was used, for example, in studies of the smooth distortion of a defect-free nematic solution of PBZT to determine certain parameters in the constitutive equation for nematic fluids.[31] If placed in an external magnetic field aligned in the plane of the sample, and along the extrusion direction, the loop defects observed in the final stage of texture evolution distort and elongate along the field. The loop will return to something close to its original shape after the magnetic field is removed, except under the following conditions. In some cases, the exposure will result in
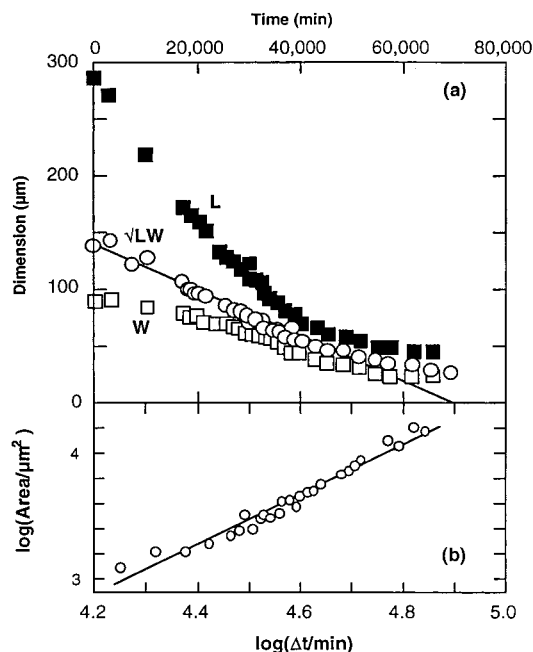
Figure 8. Relaxation of the area of a typical loop near a cell surface. (a) Relaxation of the length L (filled squares), the width W (unfilled squares) and their geometric mean $(LW)^{1/2}$ (circles) of a nearly ellipsoidal loop, with $(LW)^{1/2}$ extrapolating to zero for 70 000 min. (b) Relaxation of the area A as a function of Δt, with a disappearance time of 70 000 min. The solid line is a least-squares fit, giving $A \propto \Delta t^2$.

extended portions of the loop that are nearly linear (along the field direction), and relatively close and parallel to each other (e.g., separated by $10-20$ μm, which amounts to $1-3$ diameters of the line defect core as visualized in the microscope). Examples of the latter are given in Figures 9 and 10, showing the distortion observed after 30 min in a 2.35 T field for a sample of PBZT ($L_w = 120$ μm; $w = 0.0431$). In such cases, on relaxation following removal of the magnetic field, these nearly parallel lines move together, and form a thick, diffuse straight line, which then disappears, as one might expect for a type $s = 1$ line, via the "escape to the third dimension" mechanism.[50-53] This leaves two loops in the place of the single larger loop, which continue to diminish in area as described in the preceding section. This type of interaction has also been observed between two separate, but nearby loops after each was elongated in an external magnetic field. The example in Figure 10 shows a two-step process, in which each of two regions in which the lines of the separate loops were made essentially parallel in the field parallel merge. The schematics shown correspond to the field of view as photographed; the assignment of loop sections given in Figure 10 was abetted by wider views obtained in $x-y$ translation of the stage. The first step results in one large loop, and the second in two smaller loops, each comprising sections of the original two loops.

By contrast with the above, thick, diffuse loops, elongated in the applied field directions, are formed if a defect-free monodomain is placed in an external magnetic field, aligned in the sample plane, but orthogonal to the director.[13,32] In this case, the two essentially parallel portions of the loops, about 10 μm apart, do not merge, and in fact, the loops do not relax at all over a period of 2 years. Dichroism suggests a different orientation of the director interior to the loops, but not exactly along the magnetic field direction.
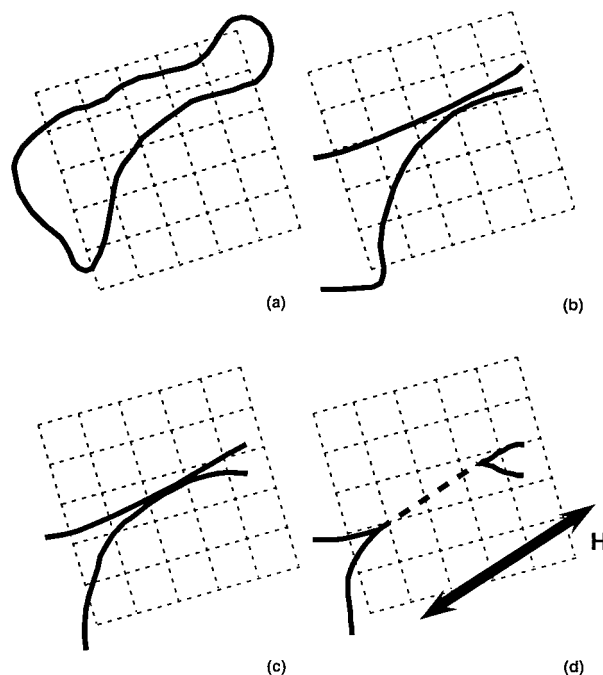
Figure 9. Relaxation of a loop in a nematic solution of PBZT following distortion in an external magnetic field oriented in the sample plane, along the director of the nematic. A schematic drawing of the initial loop on removal from the magnetic field in part a is followed by schematic drawings of the loop 5 min, 90 min, and 6 h on removal from the magnetic field in parts b−d, respectively. The dashed line in part d represents a diffuse straight line image that gradually disappeared, as the two loops continued to relax in area. The arrow gives the direction of the magnetic field orientation. 53 μm/div.

Attempt To Create a Homeotropic Alignment. Attempts to obtain homeotropic alignment have been made with nematic solutions of PPTA and PBZT by placing the sample cell in the magnetic field with the field oriented orthogonal to the cell plane. These failed no matter how soon the sample was placed into the field after extrusion or if it was heated above T_{NI} for a few hours and then cooled to room temperature in the magnetic field (7 T). When the field was removed, the sample initially exhibited a smooth texture, with weak to nil birefringence expected with a homeotropic alignment, but it also revealed some light fuzzy lines of low contrast against the smooth background. A fluorescence emission anisotropy of $I_\parallel/I_\perp \approx 2$ shows that some tendency for planar alignment remained near the confining surfaces. With increased time, $I_\parallel/I_\perp$ increased to normal levels over a period of 10^4 minutes, and the sample developed the birefringence and dichroism associated with a planar alignment. In addition, the fuzzy lines became more distinct with time, without, however, developing into clearly recognizable features, such as line defect loops. The texture, which persevered for up to 2 years, may reflect defect walls or remnants of these.

Discussion

Textural Features of the Coarsening Process. The appearance immediately after extrusion into the cell is stopped gives the illusion of domains.[13,54-56] This is attributed to a reduction of the volume v_S over which the local order parameter $S(\mathbf{r})$ is essentially constant to a volume with dimensions in the range of micrometers.[13,55,56] Presumably, within such regions $S(\mathbf{r})$ is about equal to the equilibrium order parameter S for
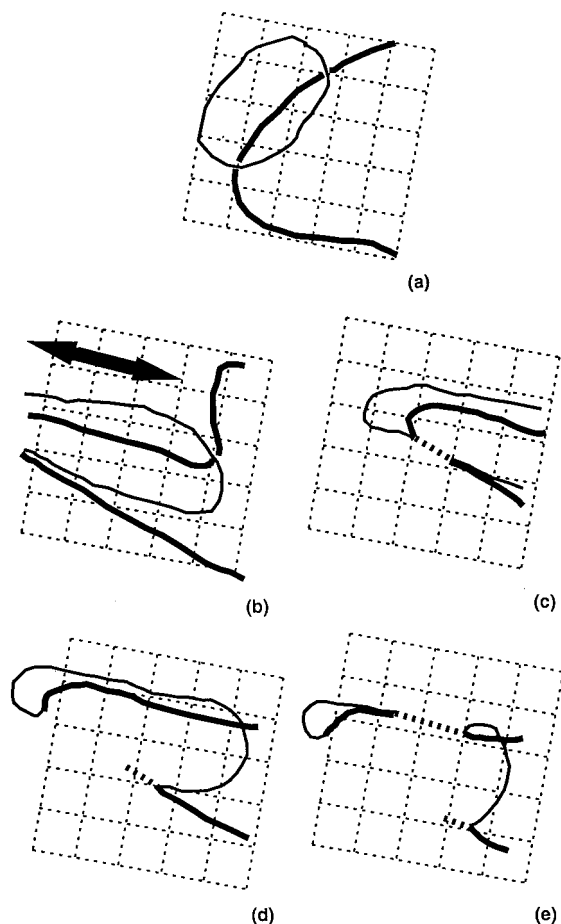
Figure 10. Relaxation of two loops in a nematic solution of PBZT following distortion in an external magnetic field oriented in the sample plane, along the director of the nematic. A schematic drawing of one of the initial loops and a portion of the other on removal from the magnetic field in part a is followed by schematic drawings of a portions of the loops 5 min, 4 h, 18.5 h, and 29.5 h on removal from the magnetic field in parts b−e, respectively. The two loops, or portions thereof, are differentiated by light and bold lines. The loops were initially displaced vertically, but were not in direct contact. 53 μm/div.

the corresponding defect-free monodomain at the same composition and temperature. However, at this early stage in the coarsening the local director field $\tilde{n}(r)$ appears to be everywhere continuous, though possibly exhibiting locally strong gradients. No features that can be identified with line defects are evident optically. The intermediate appearance of the relatively long-wave, smooth gradients in the precursor texture to the development of line defects, giving the appearance of hills and valleys in the material, further suggests the absence of a true domain structure at any stage, but instead suggests a process that gradually increases ν_S to macroscopic dimensions and suppresses gradients in the early stages of the coarsening process. The diffuse features characteristic of the precursors to line defects observed over most of the thicker cells at the early to intermediate stage of coarsening are a result of refraction in the birefringent medium. With increased coarsening, a tangle of line defects, such as that displayed in Figure 3 is observed throughout the cell, with either PPTA or PBZT, similar to the structure with small molecule nematogens.[10] Although the evolution of the tangle to leave isolated, continuous loops appears to be very similar for both PPTA and PBZT, as well as for

small molecule nematogens, the complex character of the fringe pattern associated with the tangle texture would seem to make interpretation of the behavior in terms of type $s = \frac{1}{2}$ or $s = 1$ loops, with smooth distortion of the director field from surface to surface, problematic, since such treatments assume that the twist of the director field underlying the loop occurs from each surface to the plane of the loop.[2,21,25,48,51] Thus, as demonstrated by the tendency of complex, nonplanar, and writhed loops to become planar as they decrease in size, the director field around the line defects must be very complicated and cannot generally extend from the surfaces to the plane of the loop. Similarly, the tendency of loops that writhe out of the sample plane to become planar with increasing time, as the area enclosed by the loop diminishes, along with the corresponding complexity of the fringe pattern (see Figures 4 and 5) would not be described by such models. The alternating bright and dark patterns observed along the defect loop in Figure 5, also observed with defect loops of PBZT,[13] suggest a substantial order within the loop defect itself. Any such order could take many forms; for example, a tendency for the director to be orthogonal to the axis of the line defect, but twisting periodically about that axis would give the observed behavior. The properties of the line and their effect on the adjacent director field are likely implicated in the observation that a given loop never is in contact with itself in the absence of an external field, such as the magnetic field discussed below.

As might be reasonable, the nematic near the boundaries (within 50−100 μm) appears to be more strongly aligned in the extrusion direction and less full of defects than that in the interior of the nematic. For example, this gives rise to the fluorescence emission behavior seen in Figure 1 and is presumed to be implicated in, if not entirely responsible for, the preferred orientation along the extrusion direction in the coarsening texture. The alignment in this region may be a result of an extensional "fountain flow" at the surface of the advancing fluid front during the extrusion of the nematic solution into the cell;[13] this material is exactly that deposited near the cell surfaces. As will be reported in part 3 of this series, it appears that flow alignment is much easier to attain with the PPTA solutions than with the PBZT solutions used in this study, perhaps explaining why similar rapid coarsening was not observed with solutions of PBZT. The value $(n_E - n_O)/c \approx 0.16$ mL/g observed for the solution of PPTA in the 100 μm cell several weeks after filling is within a factor of 2 of that given by the $3\delta(\partial n/\partial c)$ expected for full alignment,[57] using values of the molecular anisotropy δ and refractive index increment $\partial n/\partial c$ determined for dilute solutions.[42] Thus, the coarsened texture is close to an equilibrium alignment.

The absence of loop defects in the layer within 50−100 μm of the surfaces is consistent with prior observations on the nature of this region for nematic solutions of PBZT. A biaxial nematic alignment of surface layers of approximately the same thickness was inferred from the data on third harmonic generation, with a uniaxial nematic in the bulk,[34] and similar behavior has been reproduced in a model predicting the possibility of a transition from uniaxial in the bulk to biaxial near a surface in a nematic, depending on certain elastic constants.[58] Further, data in part 1 on the relaxation of director field distortions in a monodomain induced by an external magnetic field have shown that the

anchoring is stronger toward splay than twist distortions,[31] providing an additional means to stabilize a structure near a surface different from that in the bulk.

Loop Relaxation Dynamics. As emphasized by the preceding section, in the absence of an external field, the director field orientation in the matrix around the line-defect loops is complex, even at a stage for which the loops are predominantly planar and lie in planes parallel to those of the surfaces. Under these conditions, the anisotropy of the Frank curvature elasticity and the Leslie viscosities observed with PBZT[31,35] and anticipated for PPTA might not be too important, and it might be anticipated that the evolution of the loop size would be approximated by simplified nematodynamics involving the relaxation of the tension in the defect line in a viscous medium, giving the result $A(t) \propto \Delta t = t_0 - t$.[12,17,25] The dependence of the line tension on the curvature of the line makes this result similar to that for relaxation by curvature, in which every point on the loop moves toward its center of curvature with a velocity that is proportional to the local curvature.[59-62] As may be seen in Table 2, for loops observed in the bulk of nematic solutions of PPTA, $\nu \approx 1$, i.e., $A(t) \propto \Delta t = t_0 - t$, with these loops disappearing before those found near the surfaces. The observation that defect loops were nearly evenly distributed through the cell at a certain stage in the coarsening, except for the slabs within 50-100 μm of the cell surfaces, is consistent with the prediction that the energy tending to confine loops to the center of the cell is weak.[25,48] A Java Applet is available on a web site to reveal the change in shape as the area relaxes for an initial loop with any arbitrary planar, noncrossing loop relaxing by curvature.[63] The sequential shapes of a relaxing loop observed here are compared with the shapes calculated for relaxation by curvature beginning with a loop of the same initial shape in Figure 7. The calculations were carried out by loading the initial loop shape into the Java Applet, with the resulting shapes transferred for use in Figure 7. Although the Applet does not provide an accurate record of time, Δt could be inferred from the loop area since $A(t) \propto \Delta t$, for this calculation. The reasonable correspondence of the shapes during the relaxation of the loop line defect and those calculated by the model support the postulate that the relaxation of the line defect loops approximates relaxation by curvature. The deviations between the observed and calculated shapes could be caused by inaccuracy in determining and transferring the initial shape to the Applet, the anisotropic nature of the nematic environment, or the deviation from true relaxation by curvature. It should be noted that data on circular loop defects in a small molecule nematogen were observed to follow behavior with $\nu \approx 1$, with the loop disappearing within a few seconds ($t_0 < 10$ s).[9,12,63] Similarly, investigations of the relaxation velocity and curvature of loops in a thermotropic polymeric nematic have been cited to support the model of relaxation by curvature.[15] In a related treatment, the density ρ_{lin} of the lines per unit volume in the defect-full nematic at earlier times in the annealing is predicted to follow the evolution equation with $d\rho_{lin}/dt$ proportional to ρ_{lin}^2.[16] Reasonable agreement with this prediction has been reported for small molecule nematogens.[12] Although quantitative comparison is not possible without detailed information on the curvature elasticities and associated viscosities, it may be noted that the long relaxation times reported here are similar

to observations made on the gradual change in the light scattering as a nematic solution of a racemic mixture of poly(γ-benzyl-L-glutamate) and poly(γ-benzyl-D-glutamate) was allowed to coarsen.[64]

As noted above, the result $\nu \approx 1$ is consistent with the behavior expected with relaxation by curvature. However, this result also obtains qualitatively under certain conditions with a different model, based on the use of a dissipation principle to compute the relaxation of a planar twist loop confined to the midplane to a thin cell, with planar boundary anchoring.[25] Thus, although different in detail than relaxation by curvature for circular loops with radius R much smaller than the separation $2H$ of the confining surfaces, the qualitative behavior is similar, for either circular or noncircular loops, with $\nu \approx 1$, or $A(t) \propto \Delta t/\tau$, over most of the time range, where $\tau = \pi \eta_T H^2/4K$, with η_T being the twist viscosity and K the curvature elasticity in the single-constant approximation employed. On the other hand, as H/R is made smaller, the model gives $\nu \approx 2$, or $[A(t)]^{1/2} \propto \Delta t/\tau$, over most of the time range. Comparable results are predicted for noncircular loops,[25] similar to the results reported here for loops within 50-100 μm of the surface with nematic solutions of PPTA and earlier with nematic solutions of PBZT.[13] Otherwise, the shape changes are expected to be similar to those for relaxation by curvature, with one interesting difference: portions of the loop with zero curvature are still predicted to move as the shape evolves, unlike the behavior under relaxation by curvature. These results show that the director field alignment near the surfaces plays a significant role in slowing the relaxation of the loops in these systems. The fluorescence emission results cited above support the presumption of a planar alignment of the director field near the surfaces early in the coarsening process, as does the rapid annealing to a defect-free texture noted for the solution of PPTA in a 100 μm thick cell.

External Field Effects. Although all of the loops used in the analysis of the relaxation dynamics were planar, as shown in Figures 4 and 5, isolated nonplanar loops were observed at shorter times, with the loop writhing about itself in extreme cases, without even having the defect line come in contact with itself at any point. In undoing the writhe, portions of the loop could come into proximity to each other as the loop approached planarity but were not observed to come into contact, although such behavior has been reported for a small molecular nematogen.[10] The loop behaved as though it was everywhere repulsive to itself, which is likely the consequence of a complex director field alignment near the defect line, as mentioned above. Similarly, two nearby loops were never observed to cross or interact directly with each other as they relaxed. The behavior was very different for loops allowed to relax after distortion in an external magnetic field aligned along the extrusion direction (30 min in a 2.35 T field). The external field resulted in a similar alignment of the director everywhere surrounding the defect line and elongated the loop. As shown in Figure 9, during relaxation on removal of the magnetic field, portions of the elongated loop moved together, opposite to the direction expected by relaxation by curvature, and then joined and formed a wide, diffuse line, which then dissipated, leaving two separate loop defects. Similar effects are seen in Figure 10, in which the external magnetic field created elongated sections of two separate

adjacent loops. These sections joined in two steps, forming wide, diffuse line lines in each step, which then disappeared. The first step produced a single large loop, and the second step left two new loops, each formed by sections of the two original loops. The loops subsequently became planar, and their areas decreased, as with normally formed loops. Although adiabatic propagation prevents observation of any distortion in the interior of the loops using normally incident light, the failure to observe conoscopic interference images in the loop interior reveals that distortion is present prior to the exposure to the external magnetic field. It appears that the elongation of the loops in the magnetic field produces an effect similar to an extensional flow, unwinding the director and producing an alignment parallel to that in the bulk, at least in the region between two closely spaced parallel lines in the elongated structure. Without the support from the distorted director field between them, the closely spaced lines coalesce, with annihilation of the defect structure.

The elliptical structures sometimes observed in the wake of a translating bubble with nematic solutions of PPTA are similar in shape and behavior to stable loop structures observed with nematic solutions of PBZT if the coarsening nematic is placed in an external magnetic field at the stage when the texture is dominated by the diffuse precursors to tangle of line defects.[13,32] In both cases, the defect structure is found to be stable, without noticeable relaxation in size, shape, or orientation. Examples of loops observed with PBZT are given in the references cited, as observed in the otherwise defect-free, well-aligned monodomain created by the external magnetic field. Although these elliptical loops vary in size, they tend to exhibit a common ratio of the major to minor axes for a given sample, approximately 1.5−2.5 for samples studied here. The axial ratio may be fixed by a ratio of the Frank curvature elasticities. For example, in some cases the ratio of the major to minor axes of elliptical defect structures is predicted to be equal to the square root of the two elastic constants involved in the defect structure and is invariant with field strength.[65] With the structures in PBZT solutions, comparison of the dichroism of the interior and exterior of the loop showed that the alignment in the interior of the loop was orthogonal to that in the monodomain matrix. They exhibit what appears to be one or two thin line defects out the plane of the planar loop formed by two thicker curves, with the plane being elliptical in shape, with vertexes aligned along the molecular chains in the nematic, as judged from the dichroism, eg., see the images in refs 13 and 32. Orthoscopic imaging with light from a laser source revealed a fringe pattern associated with the defect loop, with the fringes parallel to the loop, and visible with either monochomatic or polychromatic light; the latter indicates that they arise over a small distance and do not involve many orders of retardation, In discussing the stable loops observed with PBZT solutions following exposure to an external magnetic field, it was proposed that the these developed only if the director gradients in the nematic were relatively smooth, with the possibility that a region with the local director essentially orthogonal to the eventual director of the monodomain could be trapped and isolated. The interaction with the magnetic field could be satisfied by rotation of the aromatic planes into the plane of containing the magnetic field lines, even though that would not represent a stable situation. Once trapped and isolated, it appears that these loops have essentially no energetically favorable pathway for subsequent relaxation. There does not appear to be any theoretical treatment of this effect. The loops observed in the wake of a translating bubble in nematic solutions of PPTA may have a similar origin in that some portion of the director is rotated by essentially ninety degrees in the plane of the sample by interaction with the flow field of the bubble, with that region subsequently becoming trapped, as with the corresponding region produced in the magnetic field.

Conclusions

The behavior reported here reveals the strong similarity of texture development and relaxation in nematic solutions of two different rodlike polymers. The final stages of the textural coarsening, in which isolated planar loops parallel to the plane of the cell surfaces decrease in area, can be understood with a model that explicitly incorporates the influence of the surface. At a somewhat earlier stage in the coarsening, with essentially isolated, planar loops throughout most of the cell, the behavior is similar to that for relaxation by curvature, in which a point on the line defect moves in a direction along the normal to the loop, in the plane of the loop, and with a velocity proportional to the local curvature. The more complex behavior observed even earlier in the coarsening process, for which a loop is nonplanar and may writhe about itself, with the director field away from line defect loops being smooth but not free of complex distortion, seems open to only qualitative interpretation with similar models. The behavior in an external magnetic field shows that the line defect loops can be distorted and caused to undergo annihilation behavior not seen if the external field is not applied. It is possible that similar effects may obtain under the action of an external stress field. As with prior work on third harmonic generation from nematic solutions of PBZT, the behavior reported here reveals that the texture near (50−100 μm) a surface is substantially different from that in the bulk of the nematic, presumably reflecting the strong tendency for the nematic to develop a planar alignment near the surface.

References and Notes

(1) Li, J. C. M.; Gilman, J. J. *J. Appl. Phys.* **1970**, *41*, 4248−56.

(2) Spruijt, A. M. J. *Solid State Comm.* **1973**, *13*, 1919−22.

(3) Geurst, J. A.; Spruijt, A. M. J.; Gerritsma, C. J. *J. Phys.* **1975**, *36*, 653−64.

(4) Kossecka, E.; deWit, R. *Arch. Mech.* **1977**, *29*, 749−67.

(5) Kleman, M.; Liebert, L.; Strzelecki, L. *Polymer* **1983**, *24*, 295−9.

(6) Orihara, H.; Ishibashi, Y. *J. Phys. Soc. Jpn.* **1986**, *55*, 2151–6.

(7) Nagaya, T.; Orihara, H.; Ishibashi, Y. *J. Phys. Soc. Jpn.* **1987**, *56*, 1898–904.

(8) Rieger, J. *Macromolecules* **1990**, *23*, 1545–7.

(9) Chuang, I.; Turok, M.; Yurke, B. *Phys. Rev. Lett.* **1991**, *66*, 2472–5.

(10) Chuang, I.; Durrer, R.; Turok, N.; Yurke, B. *Science* **1991**, *251*, 1336–42.

(11) Kilian, A. *Mol. Cryst. Liq. Cryst. Lett.* **1992**, *8*, 91–8.

(12) Chuang, I.; Yurke, B.; Pargellis, A. N.; Turok, N. *Phys. Rev. E* **1993**, *47*, 3343–56.

(13) Diao, B.; Matsuoka, K.; Berry, G. C. In *Keynote lectures in selected topics of polymer science*; Riande, E., Ed.; National Council of Scientific Research of Spain: Madrid, 1995; pp 191–218.

(14) Shehadeh, H. M.; McClymer, J. P. *Phys. Rev. Lett.* **1997**, *79*, 4206–9.

(15) Gunther, J.; Thomas, E. L.; Clingman, S.; Ober, C. K. *Polymer* **1998**, *39*, 4497–503.

(16) Wang, W.; Shiwaku, T.; Hashimoto, T. *J. Chem. Phys.* **1998**, *108*, 1618–25.

(17) de Gennes, P. G. In *Molecular Fluids*; Balian; R., Weill, G., Eds.; Gordon and Breach Science Publ.: London, 1976; pp 373–400.

(18) Ranganath, G. S. *Mol. Cryst. Liq. Cryst.* **1982**, *87*, 187–95.

(19) Surutzidis, A. I. Ph.D. Dissertation, 1989.

(20) Kilian, A.; Hess, S. *Liq. Cryst.* **1990**, *8*, 465–72.

(21) Kilian, A. *Mol. Cryst. Liq. Cryst.* **1992**, *222–223*, 57–69.

(22) Hudson, S. D.; Larson, R. G. *Polym. Prepr. Am. Chem. Soc.* **1994**, *33*, 545–6.

(23) Terentjev, E. M. *Phys. Rev. E* **1995**, *51*, 1330–7.

(24) Biscari, P.; Peroli, G. G. *Commun. Math. Phys.* **1997**, *186*, 381–92.

(25) Sonnet, A. M.; Virga, E. G. *Phys. Rev. E* **1997**, *56*, 6834–42.

(26) Gerritsma, C. J.; Geurst, J. A.; Spruijt, A. M. J. *Phys. Lett. A* **1973**, *43*, 356–8.

(27) Ranganath, G. S. *Mol. Cryst. Liq. Cryst.* **1988**, *154*, 43–53.

(28) Sunil Kumar, P. B.; Ranganath, G. S. *Mol. Cryst. Liq. Cryst.* **1989**, *177*, 131–44.

(29) Rey, A. D. In *Defects in Materials*; Bristowe, P. D., et al., Eds.; Vol. 209; Mater. Res. Soc.: Pittsburgh, PA, 1991; pp 299–304.

(30) Ranganath, G. S. *Int. J. Mod. Phys. B* **1995**, *9*, 2439–67.

(31) Part 1: Diao, B.; Berry, G. C. *Liq. Cryst.* **1997**, *22*, 225–38.

(32) Srinivasarao, M.; Berry, G. C. *Mol. Cryst. Liq. Cryst.* **1992**, *222–223*, 99–121.

(33) Mattoussi, H.; Srinivasarao, M.; Kaatz, P. G.; Berry, G. C. *Mol. Cryst. Liq. Cryst.* **1992**, *222–223*, 69–84.

(34) Mattoussi, H.; Berry, G. C.; Patterson, G. D. *J. Polym. Sci., B: Polym. Phys.* **1996**, *34*, 925–38.

(35) Se, K.; Berry, G. C. In *Reversible Polymer Gels and Related Systems*; Russo, P. S., Ed.; Advances in Chemistry 350; American Chemical Society: Washington, DC, 1987; pp 129–51.

(36) Panar, M.; Beste, L. F. *Macromolecules* **1977**, *10*, 1401–6.

(37) Smirnova, V. N.; Khanin, Z. S.; Iovleva, M. M.; Prozorova, G. E.; Potemkina, Z. I.; Volokhina, A. V.; Papkov, S. P. *Fibre Chem.* **1980**, *12*, 235–7.

(38) Iovleva, M. M.; Smirnova, V. N.; Khanin, Z. S.; Volokhina, A. V.; Papkov, S. P. *Polym. Sci. USSR* **1981**, *23*, 2048–51.

(39) Iovleva, M. M.; Prozorova, G. Y.; Smirnova, V. N.; Papkov, S. P. *Polym. Sci. USSR* **1981**, *23*, 2278–85.

(40) Gardner, K. H.; Matheson, R. R.; Avakian, P.; Chia, Y. T.; Gierke, T. D. In *Polymers for fibers and elastomers*; Arthur, J. C., Jr., Ed.; American Chemical Society: Washington, DC, 1984; pp 91–102.

(41) Rommel, H.; Foerster, G. *Macromolecules* **1994**, *27*, 4570–6.

(42) Cotts, P. M.; Berry, G. C. *J. Polym. Sci.: Polym. Phys. Ed.* **1983**, *21*, 1255–74.

(43) Arpin, M.; Strazielle, C. *Polymer* **1977**, *18*, 591–8.

(44) Arpin, M.; Strazielle, C.; Weill, G.; Benoit, H. *Polymer* **1977**, *18*, 262–4.

(45) Baird, D. G.; Smith, J. K. *J. Polym. Sci.: Polym. Chem. Ed.* **1978**, *16*, 61–70.

(46) Matsuoka, K.; Berry, G. C. *Nihon Reorojii Dakkaishi* **1996**, *24*, 75–85.

(47) Srinivasarao, M.; Berry, G. C. *J. Rheol.* **1991**, *35*, 379–97.

(48) Nehring, J. *Phys. Rev. A* **1973**, *7*, 1737–48.

(49) Santos, M. B. L.; Licinio, P. *Mol. Cryst. Liq. Cryst. Lett.* **1985**, *2*, 15–21.

(50) Cladis, P. E.; Kleman, M. *J. Phys.* **1972**, *33*, 591–8.

(51) Meyer, R. B. *Philos. Mag.* **1973**, *27*, 405–24.

(52) de Gennes, P.-G. *The physics of liquid crystals*; Clarendon Press: Oxford, U.K., 1974; p 140.

(53) Nagaya, T.; Orihara, H.; Ishibashi, Y. *J. Phys. Soc. Jpn.* **1995**, *64*, 78–85.

(54) Asada, T. In *Polymer Liquid Crystals*; Ciferri, A., Krigbaum, W. R., Meyer, R. B., Eds.; Academic Press: New York, 1982; pp 248–73.

(55) Berry, G. C. In *Theory & Applications of Liquid Crystals*; Kinderleher, J. L. E. D., Ed.; Springer-Verlag: New York, 1987; Vol. 5, pp 1–29.

(56) Berry, G. C.; Srinivasarao, M. *J. Stat. Phys.* **1991**, *62*, 1041–58.

(57) Chu, S. G.; Venkatraman, S.; Berry, G. C.; Einaga, Y. *Macromolecules* **1981**, *14*, 939–46.

(58) Biscari, B. P.; Virga, E. G. *Liq. Cryst.* **1997**, *22*, 419–25.

(59) Mullins, W. W. *J. Appl. Phys.* **1956**, *27*, 900–4.

(60) Grayson, M. A. *J. Diff. Geom.* **1987**, *26*, 285–314.

(61) Bronsard, L.; Kohn, R. V. *J. Diff. Equations* **1991**, *90*, 211–37.

(62) Sethian, J. A. *Am. Sci.* **1997**, *85*, 254–63.

(63) Sethian, J. A. Java Applet for relaxation by curvature. At URL http://http://math.berkeley.edu/~sethian/level_set.html, as of the date this paper was submitted.

(64) Wong, A. P. Y.; Wiltzius, P.; Larson, R. G.; Yurke, B. *Phys. Rev. E* **1993**, *47*, 2683–8.

(65) Brochard, F. *J. Phys.* **1972**, *33*, 607–11.

MA990807F